Hindawi
Journal of Control Science and Engineering
Volume 2023, Article ID 6909403, 11 pages
https://doi.org/10.1155/2023/6909403

Research Article

Calculation of RMS Current Load on DC-Link Capacitors for Multiphase Machine Drives under Carrier-Phase Shift Control

Zhigang Zhang,[1,2] **Pengcheng Zhang**,[1,2] **Yang Zhang**,[1] **Wenjuan Zhang**,[2] **Mengdi Li**,[2] **and Zichen Xiong**[1]

[1]*School of Electronic Information and Electrical Engineering, Hunan University of Technology, Zhuzhou 412007, China*
[2]*School of Electronic Information and Electrical Engineering, Changsha University, Changsha 410022, China*

Correspondence should be addressed to Yang Zhang; hut_zy@163.com

Received 11 July 2022; Revised 6 December 2022; Accepted 5 April 2023; Published 25 April 2023

Academic Editor: Jiehao Li

The reliability and economy of dc-link capacitors are important concerns in multiphase drive systems. Due to the parallel connection of several converters, the dc-link capacitors are subjected to a higher RMS current, and the root mean square (RMS) current of dc-link capacitors is an important reference standard to determine its lifetime, cost, and volume. In this paper, the RMS current of dc-link capacitor is calculated by using the dual Fourier integral method and the effect of carrier interleave is studied. Meanwhile, the modulation ratio, harmonic sidebands, and switching frequency are also considered. In order to optimize the reliability and economy of the multiphase drive system, a Cotes method combined with carrier-phase shifting technology (CPST) for calculating RMS current of the dc-link capacitor is proposed. The proposed method can provide optimization guidance for the design of dc-link capacitors. Finally, the analytical and experiment results are compared with the existing methods, and the experimental results verify the effectiveness of the proposed method.

1. Introduction

Nowadays, the multiphase machine is gaining more and more attention because of the advantages of low power density, flexible control, and high fault tolerance [1]. In multiphase machine drives, the multi-inverters connected on a common capacitor structure. Inevitably larger current ripples are generated in the dc-link capacitors. Naturally, the RMS current on the capacitors will significantly increase and have an effect on its thermal management, size design, and lifetime [2–4]. Therefore, it is inevitable to design a reliable and economical capacitor in a multiphase drive system.

On the one hand, the reduction of the RMS value is a very important aspect. Some researchers have focused on improving system stability and reducing the size of dc-link capacitors by reducing the current RMS value [5–9]. Taking the six-phase machine drives as an example, carrier interleaving between upper and lower inverters will reduce the dc-link current ripple [10–14]. If the interleaving angle reaches 90 degrees, the total current amplitude is reduced by nearly 50% [14]. Obviously, the RMS current of capacitors has sharply changed. Therefore, CPST can reduce the size and temperature rise in the capacitor design benchmark.

On the other hand, the accuracy of RMS current calculation needs careful attention, which influences the capacitance selection and lifetime monitoring [15]. Actually, the inverter uses different control strategies and the dc-link capacitor will bear different harmonic current [16, 17]. The calculation method of the RMS value of capacitor current has been reported in the literature, and it could be classified as two types: time domain analysis and harmonic spectrum analysis.

In time domain, three combined parameters (modulation depth, current amplitude, and phase angle) decided the RMS current together. A simple analytical expression is used to calculate the RMS current, while it possibly exists about 5% deviation compared to its actual value [18].

In frequency domain, the capacitor RMS current is calculated according to the harmonic frequency analysis, in which the harmonic components are obtained with a double

Fourier integration [17, 19, 20]. This method is clearly simple and easy to accomplish [19]. Besides, the effects on the RMS current under different modulation methods are analyzed in detail, and its analysis results were verified [17]. A polynomial interpolation integral method was used to calculate the RMS current, which could eliminate the external integral term and thus simplify the analytical modeling [20, 21]. The calculation methods have low accuracy and complicated processes in the existing literature, and there is still no paper to calculate the RMS current considering the CPST effect.

Therefore, a calculation method of RMS current is proposed for multiphase machine drives with CPST in this paper. This is sufficient to reflect the contribution of reliability and economy to the multiphase drive system [22]. Firstly, the effect of converter modulation on dc-link capacitor current is analyzed. Secondly, the double Fourier integration is obtained through the frequency spectrum analysis of capacitor current. In order to reduce the integration calculation process and improve the accuracy, an improved polynomial interpolation quadrature method (Cotes) is proposed. Finally, the RT-lab platform is used to verify the effectiveness of the proposed method under various operating conditions.

The rest of this article is organized as follows. Section 2 introduces the system and the impact of converter's modulation on capacitor current. In Section 3, an improved polynomial interpolation method using double Fourier analysis is proposed. Section 4 discusses the effect of CPST on multiphase machine drive. Section 5 gives the simulation results of the proposed method. Section 6 concludes this article.

2. Basic Theoretical Analysis

Figure 1 shows the topology of the six-phase PMSM drives with two inverters, which are connected to a common capacitor in parallel way. The uncontrolled rectifier is used to provide the power supply. The following theoretical analysis in this paper is based on this topology, and the six-phase machine is assumed to be working under a steady state. In addition, the inverter adopts the SVPWM control method.

2.1. Rectifier Output Current Analysis. The switching rule of diode rectifier bridge is natural commutation. In a switch cycle, the opening sequence of the rectifier diode is D1⟶D6⟶D2⟶D4⟶D3⟶D5. Therefore, the output current i_{rec} is composed of the dc component $I_{r,dc}$ and the sum of harmonic component i_{rn} as follows:

$$i_{rec} = I_{r,dc} + \sum_{n=6,12,18\ldots}^{\infty} i_{rn}. \tag{1}$$

Only the ac harmonic components can flow through the dc-link capacitor. Therefore, the capacitor RMS current $i_{c,rms}$ is mainly composed of the harmonic component of rectifier output.

2.2. Inverter Input Current Analysis. The dc-link current i_{inv} consists of the input current of the two inverters, including the ac component and dc component. It can be represented by

$$i_{inv} = i_{inv,ac} + i_{inv,dc}. \tag{2}$$

The dc component $i_{inv,dc}$ is supplied directly by the rectifier output, and the ac component $i_{inv,ac}$ is affected by the switching strategy of the inverter. The ac component $i_{inv,ac}$ consists of the sum of the six-phase switching currents. The switching current of each phase can be represented by the multiplication of the ac phase current and switching function $T(t)$. Therefore, the ac component $i_{inv,ac}$ can be written as

$$i_{inv,ac} = \left[i_{(u,v,w)}(t) + i_{(r,s,t)}(t)\right] \times \mathrm{T}(t). \tag{3}$$

Due to the switching behavior of the converters, the AC current can be represented by just fundamental frequency component as

$$\begin{cases} i_{(u,v,w)}(t) = \left[I_{(U,V,W)} \cos\left(\omega_{f1}t - \varphi_1 + \dfrac{2\pi\tau}{3}\right)\right], \\[2ex] i_{(r,s,t)}(t) = \left[I_{(R,S,T)} \cos\left(\omega_{f1}t - \varphi_2 + \dfrac{2\pi\tau}{3}\right)\right], \end{cases} \tag{4}$$

where $I_{(U,V,W)}$ and $I_{(r,s,t)}$ represent the individual current amplitudes in the respective phases. The fundamental frequency is defined as $\omega_{f1} = 2\pi f_{f1}$ or $\omega_{f2} = 2\pi f_{f2}$, where f_{f1} and f_{f2} are the current frequency of the upper and lower inverter ($\tau = 0, 1, 2$). φ_1 and φ_2 are the phase angles of the upper and lower inverter. τ is the phase shift angle. If the pulse width of the switch signal $T_1(t)$ is normalized to the switching period, equation (5) shows the time function in first and second sectors.

$$\begin{cases} \alpha_1 = \sqrt{3}\,M \sin\left(\omega_{f1}t\right) \Rightarrow 0 - \beta < \omega_{f1}t < \dfrac{\pi}{3}, \\[2ex] \alpha_1 = \sqrt{3}\,M \sin\left(\omega_{f1}t\right) + \sqrt{3}\,M \sin\left(\omega_{f1}t + \dfrac{\pi}{3}\right) \Rightarrow \dfrac{\pi}{3} < \omega_{f1}t < \dfrac{\pi}{3}. \end{cases} \tag{5}$$

Equation (5) is based on the time definitions of the switching states for SVM (space vector modulation) as explained in [16, 21]. The variable M is the modulation index according to

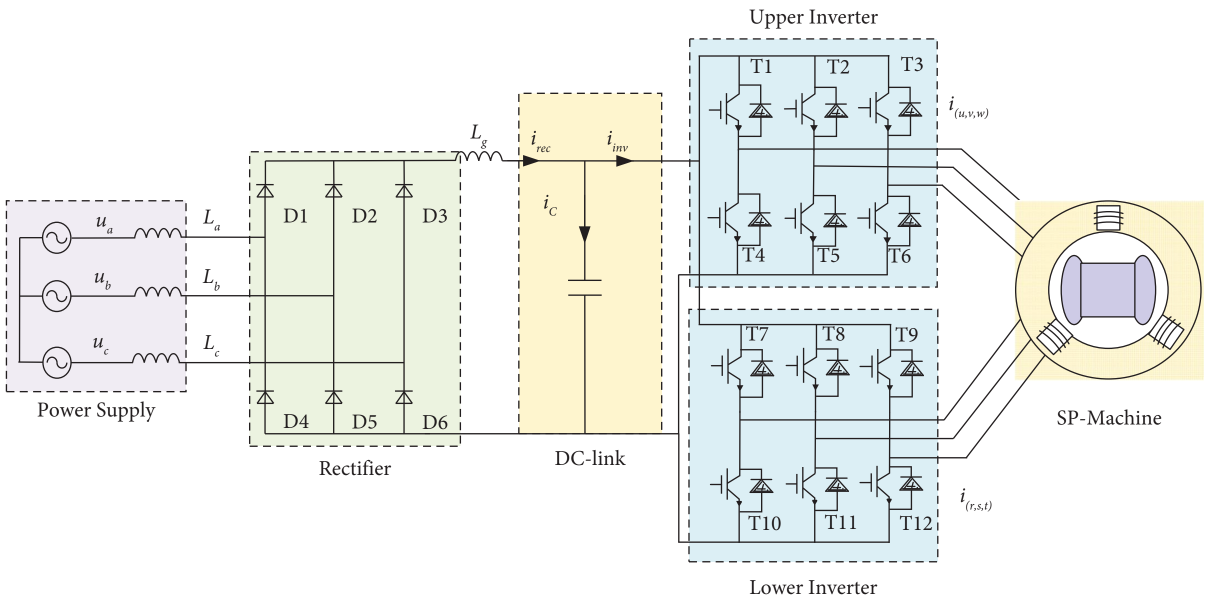

Figure 1: Topology of back-to-back converters with two inverters in parallel.

$$M = \frac{\left|U_{ref}\right|}{U_{dc}}, \tag{6}$$

where U_{ref} is the reference voltage vector. The switch signal of switch $T_7(t)$ is normalized to the switching period as

$$\begin{cases} \alpha_2 = \sqrt{3}\, M \sin\left(\omega_{f2} t\right) \Rightarrow 0 - \beta < \omega_{f2} t < \dfrac{\pi}{3} - \beta, \\ \alpha_2 = \sqrt{3}\, M \sin\left(\omega_{f2} t\right) + \sqrt{3}\, M \sin\left(\omega_{f2} t + \dfrac{\pi}{3}\right) \Rightarrow \dfrac{\pi}{3} - \beta < \omega_{f2} t < \dfrac{2\pi}{3} - \beta. \end{cases} \tag{7}$$

The angles φ of the normalized and the fundamental wave shift β are defined in Figure 2. The angle between the current time function of the U phase and fundamental wave time functions $\alpha_1(t)$ in Figure 2 is φ_1. In addition, the fundamental wave time functions $\alpha_1(t)$ and $\alpha_2(t)$ of the upper and lower inverter control strategies are shifted by an angle β.

3. Analytic Spectrum Calculation

Based on the topology in Figure 1, the RMS value of dc-link capacitor current $i_{c,rms}$ can be affected by the ac component of both rectifier output and inverter input [15]. $i_{c,rms}$ can be calculated as follows:

$$i_{c,rms} = \sqrt{i_{rec,rms}^2 + i_{inv,rms}^2}. \tag{8}$$

It can be seen that the RMS value of the inverter input current $i_{inv,rms}$ affects the $i_{c,rms}$ value. Obviously, the $i_{inv,rms}$ value is the sum of multi-inverters. For six-phase machine drives, $i_{inv,rms}$ can be represented as

$$i_{inv,rms} = i_{inv,upper,rms} + i_{inv,lower,rms}. \tag{9}$$

3.1. Description of the Current Spectrum as an Integral Function. According to Parseval's theorem, the energy of a time signal can be equal to the energy of its spectrum. Therefore, the time signal $i_{inv,upper,rms}$ can be expressed by spectrum amplitude $i_{inv,up}(f)$. As explained in [20], the upper-inverter spectrum $i_{inv,up}(f)$ results from the sum of the spectra of the three phase currents according to

$$i_{inv,up}(f) = I_u(f) + I_v(f) + I_w(f). \tag{10}$$

Furthermore, the geometric wall model method can be used to describe the switching current spectrum of the dual inverter. The method of the geometric wall model is used in [12]. Different from the analysis of switching current in time domain, the spectrum of switching current can be expressed by a double Fourier integral. Using this method, the spectrum of the inverter switch current is listed as follows:

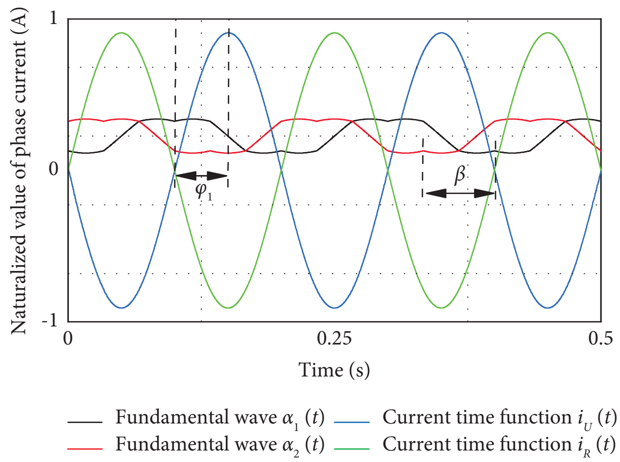

Figure 2: Naturalized value of phase current of the upper switch of phase U and R under $I_{(U,V,W)} = I_{(R,S,T)}$, $f_{?1} = f_{?2} = 50$ Hz, $\varphi_1 = \pi/2$, and $\beta = 7\pi/10$.

$$\begin{cases} I_u(f) = \dfrac{1}{2\pi^2}\left[\displaystyle\sum_{r=1}^{2}\int_{y_d(r)}^{y_u(r)}\int_{x_d(r)}^{x_u(r)} U_k e^{j(mx+ny)}dx\,dy\right], \\ I_v(f) = \dfrac{1}{2\pi^2}\left[\displaystyle\sum_{r=1}^{2}\int_{y_d(r)}^{y_u(r)}\int_{x_d(r)}^{x_u(r)} V_k e^{j(mx+ny)}dx\,dy\right], \\ I_w(f) = \dfrac{1}{2\pi^2}\left[\displaystyle\sum_{r=1}^{2}\int_{y_d(r)}^{y_u(r)}\int_{x_d(r)}^{x_u(r)} W_k e^{j(mx+ny)}dx\,dy\right], \end{cases} \tag{11}$$

where U_k, V_k, and W_k can be represented by (4), y_u, y_d, x_u, and x_d are the integration limits of the inner and outer integral, m is the carrier index variable, and n is the baseband index variable. The upper and lower limits of integration are shown in Table 1. $y = \omega_{f1}t$, $x = \omega_{sw1}t$, and $f = 1/2\pi(m\omega_{sw1} + n\omega_{f1})$, with $m, n \in N$.

As explained in Figure 2, the normalized switch functions α_1 and α_7 are shifted by the angle β. Similar to the representation of $i_{inv,up}(f)$, the spectrum of the lower inverter $i_{inv,low}(f)$ can be derived with (11) and the results are as follows:

$$\begin{cases} I_r(f) = \dfrac{1}{2\pi^2}\left[e^{j(Gg+h\beta)}\displaystyle\sum_{r=1}^{2}\int_{y_d(r)}^{y_u(r)}\int_{x_d(r)}^{x_u(r)} R_k e^{j(mx+ny)}dx\,dy\right], \\ I_s(f) = \dfrac{1}{2\pi^2}\left[e^{j(Gg+h\beta)}\displaystyle\sum_{r=1}^{2}\int_{y_d(r)}^{y_u(r)}\int_{x_d(r)}^{x_u(r)} S_k e^{j(mx+ny)}dx\,dy\right], \\ I_t(f) = \dfrac{1}{2\pi^2}\left[e^{j(Gg+h\beta)}\displaystyle\sum_{r=1}^{2}\int_{y_d(r)}^{y_u(r)}\int_{x_d(r)}^{x_u(r)} T_k e^{j(mx+ny)}dx\,dy\right], \end{cases} \tag{12}$$

where R_k, S_k, and T_k can be represented by (4). $y = \omega_{f2}t$, $x = \omega_{sw2}t$, and $f = 1/2\pi(g\omega_{sw2} + h\omega_{f2})$, with g, $\mathrm{h} \in \mathrm{N}$.

3.2. Simplified Analytical Modeling for the Calculation of the Spectrum. The expressions given in equations (11)-(12) are elementary integrals which involves many unsolved integrals. In order to obtain a simplified calculation expression, a Cotes method is carried out for the expression (11)-(12). The Cotes method is based on the idea of interpolating the original function [22]. For example, the Newton 3/8 formulas are numerical quadrature formulas for the approximate determination of an antiderivative of a function. Within the considered area, the locations of the required sampling points are in equidistant intervals. For the integral of the resulting function, an exact solution can be generated, and equations (11)-(12) are the double Fourier summation integral, which has a huge and tedious amount of calculation. Using the proposed Cotes interpolation quadrature method can eliminate a lot of the integration calculation process, and it also has a high calculation accuracy.

However, the number of sampling points in Newton rule is relatively small, resulting in a low accuracy of approximate results. Therefore, in order to obtain an approximate solution with higher accuracy, the Cotes method is proposed in this paper to simplify the calculation formula (11)-(12). The results based on the Cotes rule are presented below.

Firstly, the inner integral term in (11)-(12) is solved, as follows:

$$\begin{aligned} D(y) &= \int_{x_d(r)}^{x_u(r)} (U,V,W)_k e^{j(mx+ny)}dx \\ &= I_{(U,V,W)}\cos\left(y - \varphi_1 + \frac{2\pi\tau}{3}\right)\cdot e^{jyn}\cdot\left[-\frac{j}{m}\cdot e^{jxn}\right]_{x_d}^{x_u}, \end{aligned} \tag{13}$$

where (U, V, W) corresponds to $\tau = (1, 2, 3)$. Then, the results of applying the Cotes rule are as follows:

$$\begin{aligned} i_{inv,up}(f) &= \frac{1}{2\pi^2}\cdot I_{(U,V,W)}\cdot\sum_{r=1}^{2}\int_{y_d(r)}^{y_u(r)} D(y)dy \\ &\approx \frac{1}{2\pi^2}\cdot I_{(U,V,W)}\cdot\sum_{r=1}^{2}\int_{y_d(r)}^{y_u(r)} C(y)dy \\ &= \frac{1}{2\pi^2}\cdot I_{(U,V,W)}\sum_{r=1}^{2}\left[y_u(r) - y_d(r)\right]\cdot\sum_{k=1}^{5} Q_k\cdot D(s_k). \end{aligned} \tag{14}$$

Here, $C(y)$ represents the function approximated to the original function. The coefficient Q_k represents the weights, which can be found in Table 2. The coefficient s_k describes the location of the steps and is defined as

$$s_k = y_d + z_k\left[y_u(r) - y_d(r)\right]. \tag{15}$$

Hence, $k \in \{1, 2, 3, 4, 5\}$. The variable z_k represents the normalized location of the steps, which can also be found in Table 2. It can be seen that this solution does not contain any integral or differential expressions. Therefore, the Cotes method has more simplified calculation accuracy and the process.

Table 1: Integration limits for the double Fourier integral of switch current.

r	$Y_d(r)$	$Y_u(r)$	$X_d(r)$	$X_u(r)$
1	0	$\pi/3$	$\pi/2(1-\alpha_1)$	$3\pi/2(1+\alpha_1/3)$
2	$\pi/3$	$2\ \pi/3$	$\pi/2(1-\alpha_1)$	$3\pi/2(1+\alpha_1/3)$

Table 2: Sampling points and weight coefficients.

k	1	2	3	4	5
Q_k	0.078	0.36	0.13	0.36	0.078
Z_k	0	0.25	0.5	0.75	1

Similarly, $I_{(r,s,t)}(f)$ can be described. The sum of $I_u(f)$ to $I_t(f)$ then defines the total spectrum $i_{inv}(f)$. An approximate description of the total spectrum $i_{inv}(f)$ takes into account the first six harmonics and their sidebands. In the case of odd harmonics, the sidebands are around $\pm 3f_f$, and for even harmonics, they occur around $\pm 6f_f$. Equation (16) can be obtained from this rule.

$$I_{inv,rms} \approx \sqrt{\sum_{n\in(-3;0;3)} \sum_{m\in(1;3;5)} \left[\left|I_{inv}(f)\right|\right]^2 + \sum_{n\in(-6;0;6)} \sum_{m\in(2;4;6)} \left[\left|I_{inv}(f)\right|\right]^2}. \tag{16}$$

4. Influence of CPST on the RMS Value of Capacitive

Compared to the analysis method in the time domain, it is easier to explain the principle of interleaving in the frequency domain. According to equations (11)-(12), the fundamental wave displacement β is not considered, and the difference between $i_{inv,up}(f)$ and $i_{inv,low}(f)$ is determined by G. As shown in the following equation,

$$i_{inv}(f) = i_{inv,up}(f) + i_{inv,low}(f) = i_{inv,up}(f)\cdot\left(1+e^{jgG}\right). \tag{17}$$

Obviously, the $i_{Inv}(f)$ is maximum when the switching cycle clock signal without interleaving. $i_{inv}(f)$ is going to decrease by selecting an appropriate displacement angle G within [0-2π]. According to (8) and (17), $i_{c,rms}$ can be reduced by CPST. The switching cycle shift is the angle between the control signals from the upper inverter and lower inverter [23], as shown in Figure 3.

5. Verify the Validity of the Proposed Method

In order to verify the effectiveness of the proposed method, we used the RT-lab experimental platform for verification. All the experiment data are obtained by using the RT-LAB experiment platform, and the RT-LAB experiment platform is shown in Figure 4. The RT-LAB can implement the hardware in the loop simulation (HILS) for the six-phase machine drive system. The model of the DSP controller is TMS320F2812, which runs the algorithm, and RT-LAB (OP5600) is used to construct other parts of the system such as the six-phase machine and dual inverter.

The system parameters are shown in Table 3. The switching frequency and control frequency are both 4 kHz. The phase currents are considered as ideal cosine functions. The amplitude of the input three-phase voltage is 326 V, and the machine operation frequency is 50 Hz.

Figure 5 shows the dc-link capacitor current before and after the CPST method. To make it a fair comparison, the parameters of the drive system are strictly the same. It can be seen from Figure 5 that the capacitor current ripple is significantly reduced using the CPST method. Besides, the amplitude of current ripple decreases obviously. Therefore, Figure 5 shows that CPST has an inhibitory effect on the RMS value of the dc-link capacitor current.

5.1. Verification of the Effect of CPST by the Experiment. As described in previous sections, the RMS value of dc-link capacitor current could be reduced by the CPST. As can be seen from equations (11)-(12), $i_{inv}(f)$ is highly correlated with variables M, G, and β. Figure 6 shows the spectrum analysis of i_{inv} under different conditions of the modulation index M and the displacement angle $G = 0$ and $G = 90°$, and the variable β is considered to be the constant zero.

In order to verify the effect of CPST, the experiments for dual-three phase machine are performed, and the system models were loaded into RT-lab, respectively, to observe the effect of dc-link capacitor current. Figure 6 shows that the

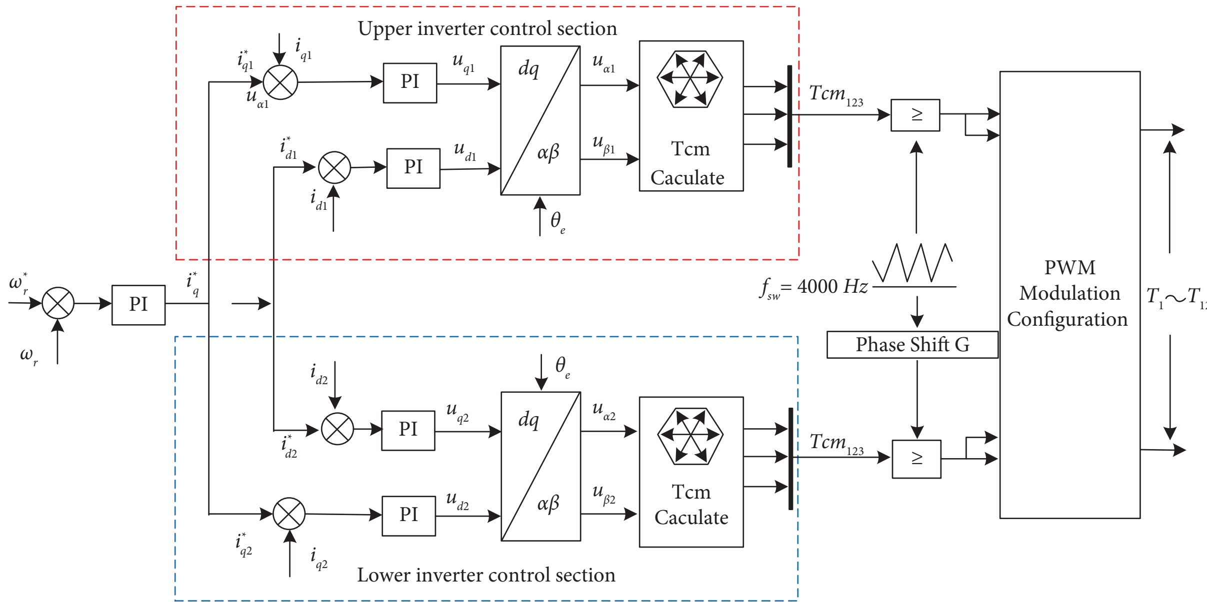

Figure 3: CPST control algorithm unit.

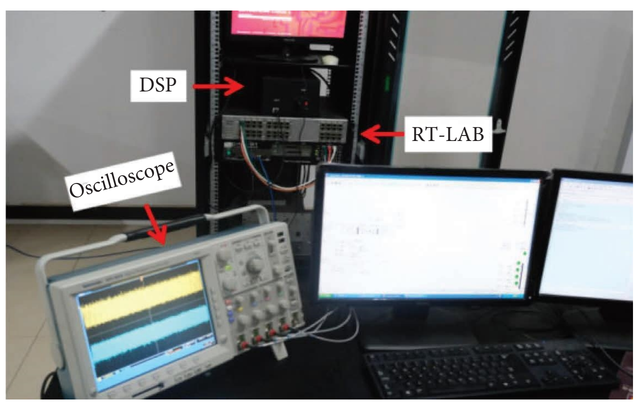

Figure 4: RT-LAB experiment platform.

Table 3: Key simulation parameters of the multiphase machine drives system.

Parameters	Values	Units
R_s	0.9	Ω
L_d/L_q	0.018	H
J	0.001	$kg \cdot m^2$
P	4	poles
Ψ_f	0.445	Wb
Dc-link L_g	0.00125	H
Dc-link C	680	uF

results of the capacitor current FFT analysis using CPST at three different modulation ratios 1, 0.8, and 0.5. The results show that the proposed CPST method could reduce the 2 fs harmonics effectively at various modulation ratios, and the diminution of 2 fs harmonics current is the main reason of dc-link capacitor RMS current reduction.

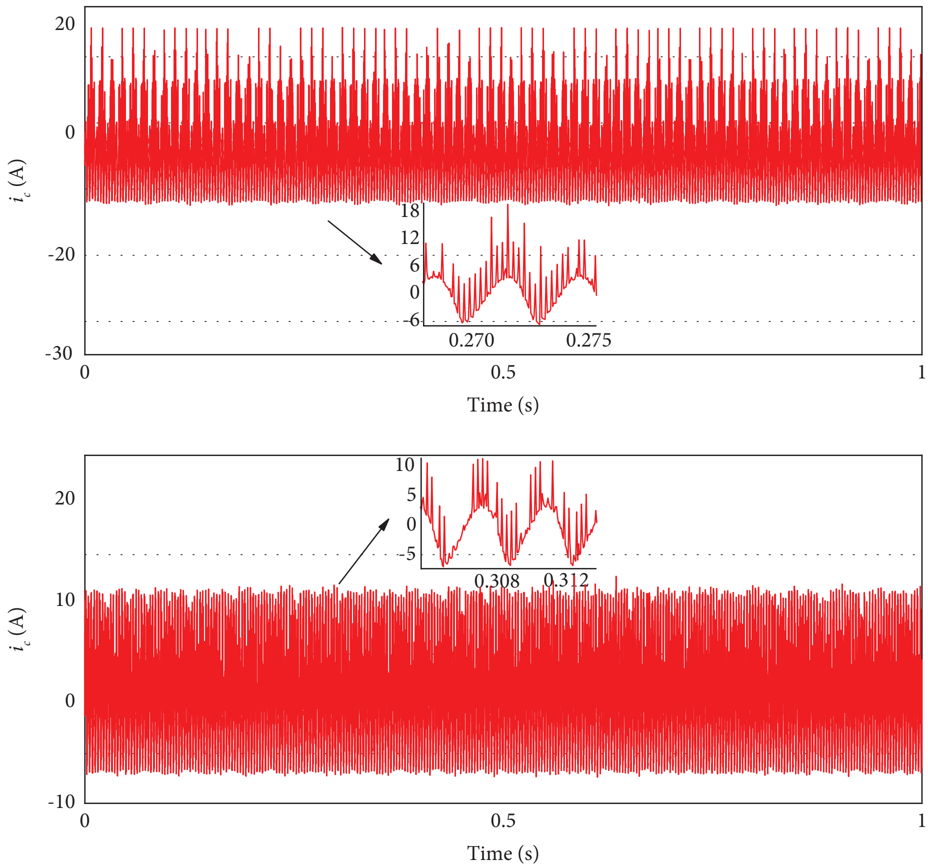

Figure 5: Capacitive current comparison of the dc-link before and after the phase shift.

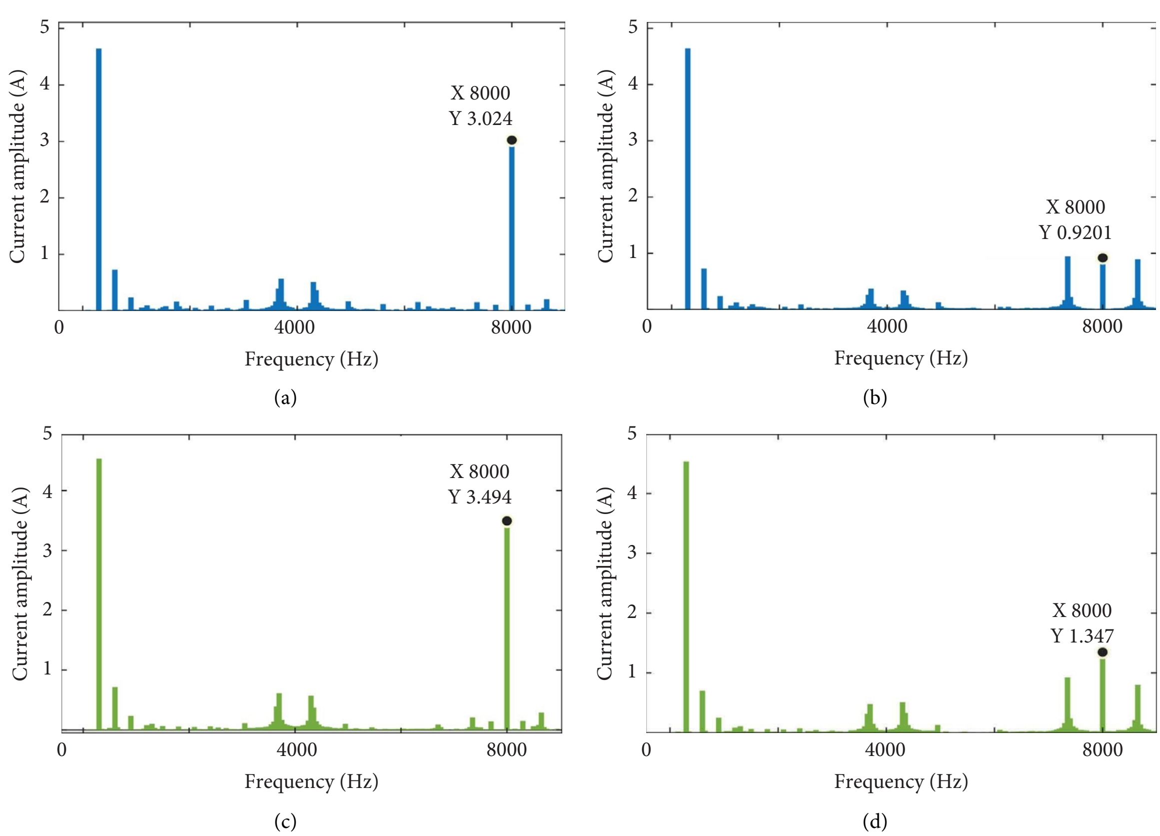

Figure 6: Continued.

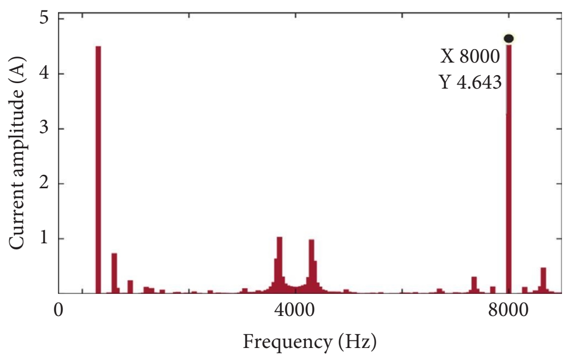

(e)

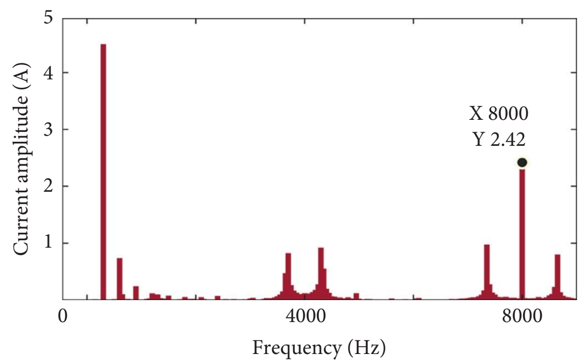

(f)

Figure 6: MATLAB FFT analysis of dc-link capacitive current under various modulation: (a) $M = 1$, $G = 0^\circ$, (b) $M = 1$, $G = 90^\circ$, (c) $M = 0.5$, $G = 0^\circ$, (d) $M = 0.5$, $G = 90^\circ$, (e) $M = 0.8$, $G = 90^\circ$, and (f) $M = 0.8$, $G = 90^\circ$.

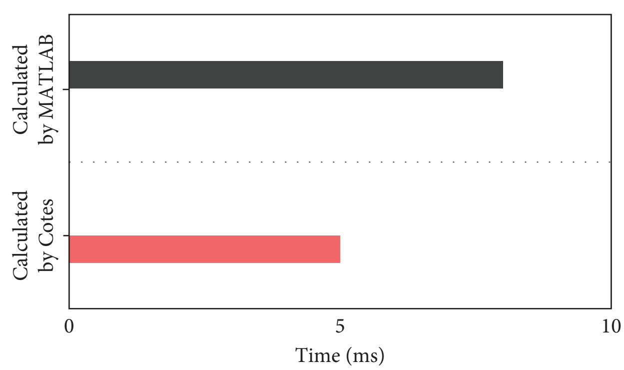

Figure 7: Comparison of calculation time of the double integral and Cotes interpolation integral.

5.2. Verification of the Approximate Effect of the Cotes Rule by Calculation. In order to verify the simplification of the Cotes method, a comparison experiment of the calculation speed is established, such as the Cotes method and MATLAB double Fourier calculation method. Equations (11)-(12) can be computed in two different ways. The programs of the two calculation methods are executed by the DSP controller (TMS320F2812), and the execution time is recorded by inserting breakpoints. Figure 7 shows the comparison result of calculation speed. The program execution time of the Cotes method is about 5 ms, and the MATLAB FFT method is about 8 ms. From the results, we can see that the Cotes method is about 30% faster. Therefore, the proposed Cotes method is more simplified.

In order to verify the effectiveness of the proposed method, the results of two approximate methods are compared, considering the carrier index m. Equations (11)-(12) define the original function, which are applied to the Newton 3/8 method proposed in literature [20] and the Cotes method proposed in this paper. Then, the standard integral calculation method in [17], the approximate results of the Cotes method, and Newton 3/8 method are compared.

In order to verify the accuracy of the proposed Cotes method, three different methods (Newton 3/8, FFT analysis, and the proposed method) are used to calculate the RMS value of dc-link capacitor current. Figure 8 shows the RMS value of the dc-link capacitor current $I_{c,rms}$ as a function of M for different 1–6 times the switching frequency (after CPST). The black line represents the calculation results of the method proposed in [17], the red line represents the calculation results of the method proposed in [20], and the blue line represents the calculation results of the method proposed in this paper. The high precision of the Cotes method is proved by the graphic results. Comparing the three methods, the Cotes method proposed in this paper has a better approximation degree than the MATLAB FFT analysis method. Therefore, the higher calculation accuracy

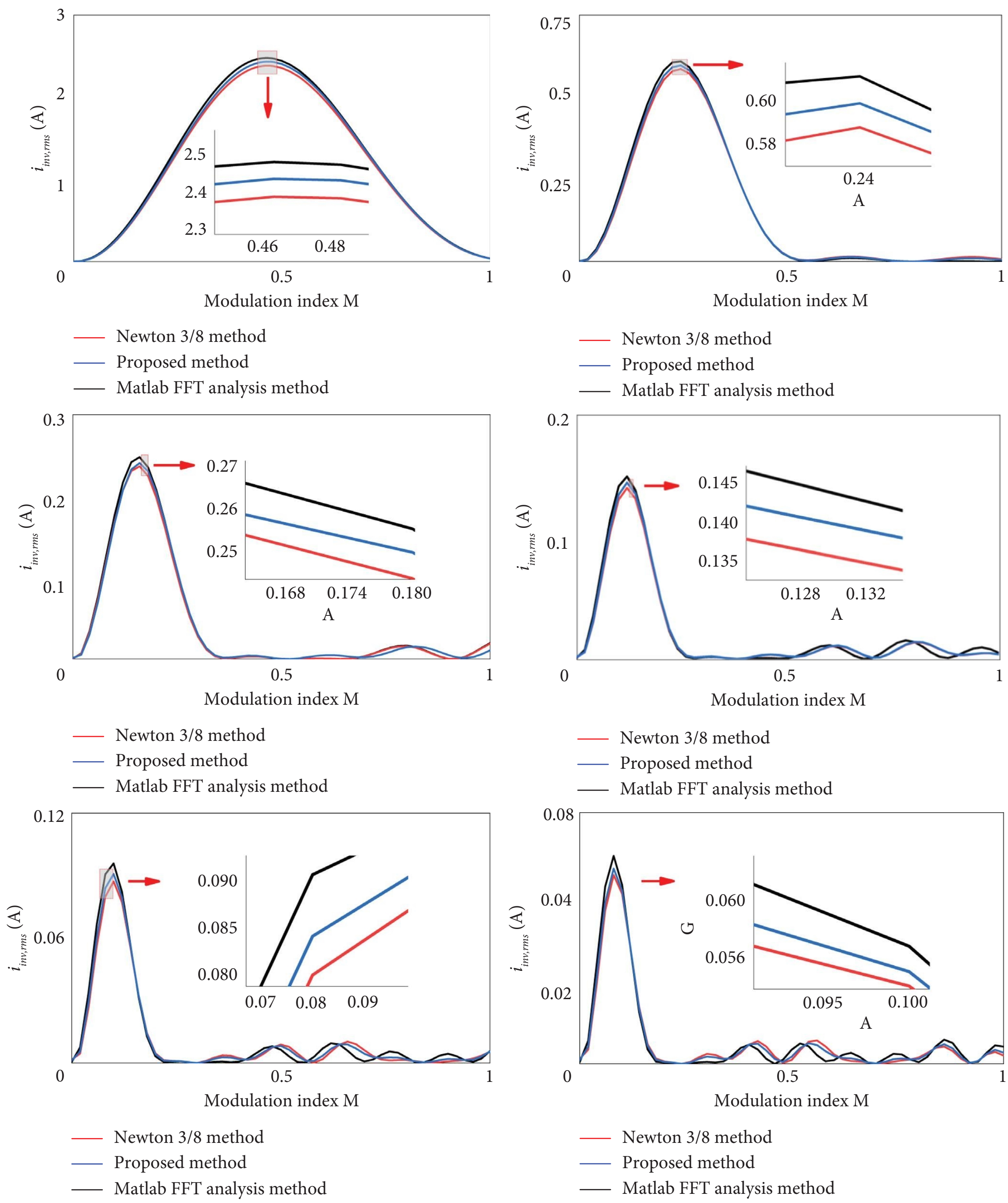

FIGURE 8: The approximate accuracy of the Cotes method is shown by calculating the amplitudes of the harmonics of six frequencies.

and simplified calculation process of the Cotes method are confirmed.

Figure 9 shows the calculation error of comparison results between the Newton 3/8 rule and Cotes rule calculated spectrum for the switch frequency. The calculated results are 7.021 A and 7.101 A, respectively, under two different methods, and the proposed Cotes method is more similar to the MATLAB FFT calculation results. Therefore, the error of the Cotes method is less than that of the Newton 3/8 rule method.

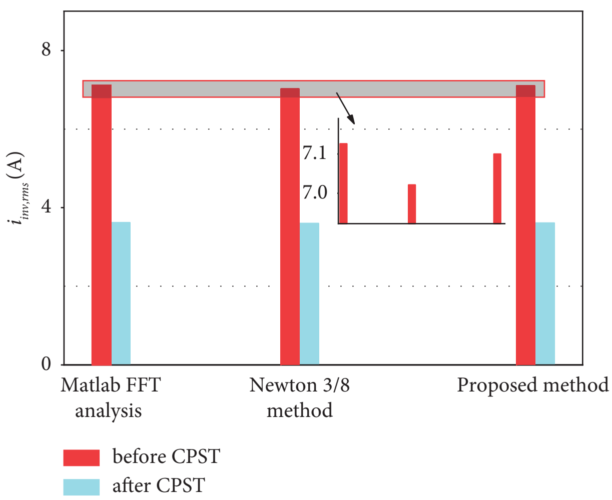

Figure 9: Calculation error comparison between the Newton method and proposed method before and after CPST.

6. Conclusions

In this paper, a new calculation expression of the RMS value of dc-link capacitor current is given in the six-phase machine drive. Compared with existing methods, a simplified form of calculation is obtained. This method calculates the integral by using the idea of polynomial interpolation, which not only reduces the calculation process but also improves the accuracy of calculation results. Therefore, the simplified calculation method of the capacitor current RMS value is combined with the CPST method, which lays a foundation for the optimal design of dc-link capacitor cost, volume, and service life.

Data Availability

The data used to support the findings of this study are included within the article.

Conflicts of Interest

The authors declare that there are no conflicts of interest regarding the publication of this paper.

Acknowledgments

This work was supported by the Key Projects of Scientific Research of the Hunan Provincial Education Department (22A0603), major special projects of the Changsha Science and Technology Plan (kq2105001), and the National Natural Science Foundation of China (51907061)

References

[1] M. Lu, D. Zhang, B. Xu, H. Yang, and Y. Xin, "Multiphase SVPWM strategy analysis and implementation of seven-phase permanent magnet synchronous motor," *Complexity*, vol. 2020, Article ID 8854472, 12 pages, 2020.

[2] M. S. Bilgin, G. Poyrazoglu, and M. Aktem, "Dc-link capacitor lifetime under various operating conditions," in *Proceedings of the 2019 IEEE 13th International Conference on Compatibility, Power Electronics and Power Engineering (CPE-POWERENG)*, pp. 1–6, Sonderborg, Denmark, April 2019.

[3] M. E. Meral and D. Elik, "Mitigation of DC-link voltage oscillations to reduce size of DC-side capacitor and improve lifetime of power converter," *Electric Power Systems Research*, vol. 87, no. 8, pp. 2491–2499, 2021.

[4] S. S. Ahmad and G. Narayanan, "Evaluation of dc-link capacitor rms current in switched reluctance motor drive," *IEEE Transactions on Industry Applications*, vol. 57, no. 2, pp. 1459–1471, 2021.

[5] K. S. Gopalakrishnan and G. Narayanan, "Space vector based modulation scheme for reducing capacitor RMS current in three-level diode-clamped inverter," *Electric Power Systems Research*, vol. 117, no. 12, pp. 1–13, 2014.

[6] X. Lyu, Y. Li, and D. Cao, "Dc-link RMS current reduction by increasing paralleled three-phase inverter module number for segmented traction drive," *IEEE Journal of Emerging and Selected Topics in Power Electronics*, vol. 5, no. 1, pp. 171–181, 2017.

[7] Y. Yang, P. Davari, F. Zare, and F. Blaabjerg, "Enhanced phase-shifted current control for harmonic cancellation in three-phase multiple adjustable speed drive systems," *IEEE Transactions on Power Delivery*, vol. 32, no. 2, pp. 996–1004, 2017.

[8] Y. Qi, J. Fang, J. Liu, and Y. Tang, "Coordinated control for harmonic mitigation of parallel voltage-source inverters," *CES Transactions on Electrical Machines and Systems*, vol. 2, no. 3, pp. 276–283, 2018.

[9] L. Zhou, W. Wu, Y. Chen et al., "Harmonic voltage distortion damping method for parallel connectedLCL-type inverters in islanded operation," *IEEE Transactions on Industrial Electronics*, vol. 66, no. 11, pp. 9032–9044, 2019.

[10] M. Schiedermeier, C. Rettner, M. Steiner, and M. M¨arz, "Dual-inverter control synchronization strategy to minimize the Dc-link capacitor current," in *Proceedings of the 2020 IEEE Vehicle Power and Propulsion Conference (VPPC)*, pp. 1–6, Gijon, Spain, November 2020.

[11] Z. Quan and Y. Li, "Impact of carrier phase shift PWM on the DC-link current of single and interleaved three-phase voltage source converters," in *Proceedings of the 2017 IEEE Energy Conversion Congress and Exposition (ECCE)*, pp. 3851–3855, Cincinnati, OH, USA, October 2017.

[12] D. Zhang, F. Wang, R. Lai, T. Thacker, and D. Boroyevich, "Interleaving impact on harmonic current in DC and AC passive components of paralleled three-phase voltage-source converters," in *Proceedings of the 2008 Twenty-Third Annual IEEE Applied Power Electronics Conference and Exposition*, pp. 219–225, Austin, TX, USA, February 2008.

[13] J. C. Kartick, B. K. Sujit, and K. C. Suparna, "Dual reference phase shifted pulse width modulation technique for a N-level inverter based grid connected solar photovoltaic system," *IET Renewable Power Generation*, vol. 10, no. 7, pp. 928–935, 2016.

[14] S. Baburajan, H. Wang, D. Kumar, Q. Wang, and F. Blaabjerg, "Dc-link current harmonic mitigation via phase-shifting of CarrierWaves in paralleled inverter systems," *Energies*, vol. 14, p. 4229, 2021.

[15] H. Wang, S. Huang, D. Kumar et al., "Lifetime prediction of DC-link capacitors in multiple drives system based on simplified analytical modeling," *IEEE Transactions on Power Electronics*, vol. 36, no. 1, pp. 844–860, 2021.

[16] N. Rouhana, E. Semail, and J.-F. Duguey, "Impact of PWM strategies on RMS current of the dc-link voltage capacitor of a dual-three phase drive," in *Proceedings of the 2014 IEEE*

Vehicle Power and Propulsion Conference (VPPC), pp. 1–7, Coimbra, Portugal, October 2014.

[17] M. H. Bierhoff and F. W. Fuchs, "Dc-link harmonics of three-phase voltage-source converters influenced by the pulsewidth-modulation strategy—an analysis," *IEEE Transactions on Industrial Electronics*, vol. 55, no. 5, pp. 2085–2092, 2008.

[18] J. W. Kolar, T. M. Wolbank, and M. Schrodl, "Analytical calculation of the RMS current stress on the DC link capacitor of voltage DC-link PWM converter systems," in *Proceedings of the 1999 Ninth International Conference on Electrical Machines and Drives*, pp. 81–89, New York, NY, USA, July 1999.

[19] J. F. Moynihan, M. G. Egan, and J. M. D. Murphy, "Theoretical spectra of space-vector-modulated waveforms," *IEE Proceedings - Electric Power Applications*, vol. 145, no. 1, pp. 17–24, 1998.

[20] M. Schiedermeier, F. Schlamp, C. Rettner, and M. Marz, "Analytical calculation of the RMS value and the spectrum of the dc-link current of a dual-inverter," *IEEE Transactions on Power Electronics*, vol. 37, no. 1, pp. 782–794, 2022.

[21] A. Voldoire, "Analytical Calculation of Dc-link Current for N-Interleaved 3-Phase PWM Inverters Considering AC Current Ripple," in *Proceedings of the 2019 21st European Conference on Power Electronics and Applications*, pp. 1–10, Genova, Italy, September 2019.

[22] P. Sundararajan, M. H. M. Sathik, F. Sasongko, C. S. Tan, M. Tariq, and R. Simanjorang, "Online Condition Monitoring System for DC-Link Capacitor in Industrial Power Converters," *IEEE Transactions on Industry Applications*, vol. 54, no. 5, pp. 4775–4785, 2018.

[23] Z. Zhu, S. Wang, B. Shao, L. Yan, P. Xu, and Y. Ren, "Advances in dual-three-phase permanent magnet synchronous machines and control techniques," *Energies*, vol. 14, no. 22, p. 7508, 2021.

[24] S. Zhang, S. Ray, R. Lu, and Y. Zheng, "Efficient learned spatial index with interpolation function based learned model," *IEEE Transactions on Big Data*, vol. 9, no. 2, pp. 733–745, 2023.

[25] B. R. Hunt, "Spectral Effects in the Use of Newton—Cotes Approximations for Computing Discrete Fourier Transforms," *IEEE Trans Comput*, vol. 20, no. 8, pp. 942-943, 1971.